



TECHNICAL ARTICLE

Effect of Aging on Pitting Corrosion Resistance of 21Cr Lean Duplex Stainless Steel with Different Molybdenum Contents

Byung-Jun Yoon and Yong-Sik Ahn

Submitted: 11 January 2022 / Revised: 22 August 2022 / Accepted: 25 September 2022 / Published online: 12 October 2022

The effects of aging heat treatment on localized corrosion behavior in lean duplex stainless steel with 0-2% Mo were investigated. The cold-rolled samples were solution-treated at 1050 °C for 5 min, and during subsequent aging at 700 °C, precipitation of a secondary phase occurred at the α -phase interior and/or the α/γ -phase boundary; this precipitate was confirmed as Cr_2N . Less Cr_2N was precipitated with increasing Mo content than with increasing aging time. The pitting potential (E_{pit}) and critical pitting temperature values decreased drastically, even after 5 min of aging time, compared with the as-solutionized steel; the values decreased with aging time. This behavior was likely caused by the depletion of Cr and N components related to precipitation of Cr_2N at the α/γ -phase boundary.

Keywords aging, duplex stainless steel, Mo addition, pitting corrosion

1. Introduction

Duplex stainless steel (DSS) is composed of dual-phase structures with ferritic (α) and austenitic (γ) phases and exhibits better combination of mechanical properties and corrosion resistance compared with single-phase stainless steels (Ref 1-3). DSSs are conventionally high-alloy steels in which the equilibrium-phase fractions depend on the alloying elements. Various secondary phases formed during the heat treatment of DSS deteriorate its mechanical properties and corrosion resistance. The typical secondary phase of DSS is known as the σ -phase, which occur during heating in a specific temperature range (Ref 4). Some recent works (Ref 5-7) where the effect of heat treatments on the corrosion and mechanical properties of DSS is studied regarding precipitation of the sigma phase.

The σ -phase precipitation can be promoted by the addition of Cr and Mo elements (Ref 8-11), and arises from the decomposition of the ferrite phase, which is closely associated with the formation of chromium nitride (mostly Cr_2N) precipitates (Ref 12-15). DSS is more expensive than 300-series austenitic stainless steel with similar corrosion resistance. Hence, lean DSS containing reduced Ni and Mo contents has been extensively studied (Ref 16, 17). Molybdenum improves

pitting and corrosion resistance; therefore, most types of DSS contain Mo element. The addition of Mo improves pitting resistance by thickening the passive film (Ref 18-21) and improves surface repassivation properties (Ref 22-24). However, when a large amount of Mo is present, the secondary phase can be easily precipitated during annealing or cooling, which is a major concern because it causes embrittlement and deteriorates corrosion resistance (Ref 25). Research has been conducted to reduce the content of the expensive Mo element while maintaining corrosion resistance and mechanical properties (Ref 26-30). However, there have been few reports concerning corrosion resistance related to formation of the secondary phase in lean DSS as a function of Mo content and aging treatment. It is very important to understand the pitting corrosion behavior in lean DSS with different molybdenum content.

The microstructural evolution of lean DSSs with Mo contents of 0-2 wt.% after aging treatment at 700 °C was investigated in this study, and the pitting corrosion resistance of the steels was compared with regard to precipitation of the secondary phase. Thus, the effect of Mo addition on the precipitation of second phase and consequently the pitting corrosion was discussed.

2. Experimental

21Cr lean DSSs with 0-2% Mo component were hot rolled followed by cold rolling into 1 mm thick plates, subsequently solution-treated at 1050 °C for 5 min, and aged at 700 °C for various intervals. Table 1 shows the chemical compositions of the steel plates, which was determined using an optical emission spectrometer (LAVM10) and an elemental analyzer (TC600; LECO). There was little difference in the results of two techniques. Hereafter, the DSS samples are referred to as 0, 1, or 2Mo steel. The solutionized steels were aged at 700 °C for 5-1200 min, then water-quenched. For microstructural obser-

The original version of this article was revised: In the originally published article, the order of authorship was incorrect. The correct author list is “Byung-Jun Yoon and Yong-Sik Ahn.”

Byung-Jun Yoon and Yong-Sik Ahn, Pukyong National University, Busan, Republic of Korea. Contact e-mail: ysahn@pknu.ac.kr.

Table 1 Chemical compositions (wt.%) of duplex stainless steels

Grade	Cr	Ni	Mn	Si	Cu	C	N	Mo	Fe
0Mo	21.10	1.00	3.62	0.71	0.78	0.028	0.19	0.02	Bal.
1Mo	21.10	1.00	3.60	0.71	0.79	0.030	0.20	1.00	Bal.
2Mo	21.20	0.99	3.70	0.71	0.79	0.029	0.22	1.93	Bal.

vation using optical microscope (OM), samples were polished and electrolytically etched (at 0.5 V for 1 min) in a nitric acid solution (60% distilled water + 40% nitric acid) using a electrolytic polishing machine (Lectropol-5; Struers).

In order to examine the influences of Mo addition and aging treatment on pitting corrosion resistance, the potentiodynamic polarization method was carried out using a Gamry Reference 600 instrument. Specimens for working electrodes were cut to the dimension of $50 \times 50 \times 10 \text{ mm}^3$, and mechanically polished to 2400 grit using SiC emery paper. The electrode potential was measured with respect to the saturated calomel electrode (SCE), and a platinum foil was used for the counter electrode. The tests were performed in a solution (3.5% NaCl) made by dissolving NaCl powder (99.6% pure) in distilled water. The electrolytes were maintained at $30 \pm 1 \text{ }^\circ\text{C}$ during tests and continuously purged with purified argon gas to deaerate the solution. The potential was anodically scanned at a rate of 0.333 mV/s from -500 mV (SCE) to the potential at which the current density exceeded $100 \mu\text{A}/\text{cm}^2$. Pitting potential (E_{pit}) was identified on the basis of the regulation of ASTM G 150.4 as the potential where the current density reached $100 \mu\text{A}/\text{cm}^2$.

To obtain the critical pitting temperature (CPT), potentiostatic tests were also performed by applying an anodic potential of 300 mV (SCE) on the specimen, with the electrolyte temperature continuously increasing at a rate of $1 \text{ }^\circ\text{C}/\text{min}$ until the current density rapidly increased. The CPT of the samples was defined by polarization curves as the temperature at which the current density continuously exceeded $100 \mu\text{A}/\text{cm}^2$ according to the standard ASTM G150. Before the test, pure nitrogen gas (N_2) was bubbled through the electrolyte to remove oxygen gas (O_2). The mean value was determined using at least five test results from potentiodynamic polarization and CPT potentiostatic tests for each sample to ensure reliability.

The α - and γ -phase contents of each sample were calculated using a commercial software (Thermo-Calc v.10) and the database (TCFE6.2); these data were then used to calculate the pitting resistance equivalent number (PREN). To observe the early stage of pit formation, specimens were mechanically polished using alumina solution with a particle size of $0.01 \mu\text{m}$, and then were immersed in a 4 mol/L NaCl + 0.01 mol/L HCl solution at $30 \text{ }^\circ\text{C}$ for 5 min. The etched specimens were observed using a field-emission electron probe microscope (FE-SEM; JSM7001F; JEOL). Field-emission electron probe microanalysis (FE-EPMA; JXA8530F; JEOL) was also used to examine the elemental distribution in the phases of α and γ . To characterize the secondary phase precipitation, a field-emission transmission electron microscope (FE-TEM; Tecnai Osiris; FEI at 200 kV) with a Z-contrast high-angle annular dark field-scanning transmission electron microscope (HAADF-STEM) was used by preparing a carbon (C) replica.

Table 2 Phase fractions of α - and γ -phases of duplex stainless steels using by Thermo-Calc data and the test results by image analyzer

	Thermo-Calc			Image analyzer		
	0Mo	1Mo	2Mo	0Mo	1Mo	2Mo
α -phase	55	68	70	56	60	65
γ -phase	45	32	30	44	40	35

3. Results and Discussion

3.1 Microstructural Evolution during Aging

Table 2 shows the α - and γ -phase contents of each sample by Thermo-Calc data and the test result to be measured using by image analyzer with optical microscope. The ferrite-phase fraction increased with Mo content, and it is overall slighter higher in Thermo-Calc data compared with the test result using image analyzer. Figure 1 shows the FE-SEM microstructure of three DSSs as a function of aging time. As shown in Fig. 1(a), the α -ferrite and γ -austenite phases are identified by light and dark colors, respectively. The white arrow at the α/γ -phase boundaries in Fig. 1(c) indicates nucleated intermetallic precipitates, and the dark spots at the α -phase interior should be pits or localized corrosion. With the increase in aging time, the amount of precipitates at the α/γ -phase boundaries increased and the size of spots grew. With the increase in Mo content, the fraction of α -phase increased and the amount of precipitates at α/γ boundaries and dark spots in α -phase decreased. A SEM micrograph and field-emission electron probe microanalysis of 1Mo steel had been aged for 60 min in which lots of secondary phases were observed at the α/γ -phase boundaries (Fig. 2). The formation of precipitates was confirmed in the phase boundary regions and is indicated by arrows. The elemental mapping analysis using FE-EPMA describes that Cr and nitrogen (N) elements were aggregated at the α/γ -phase boundary, in opposition to the findings before aging. This result implies that nitride-containing Cr has been formed through aging as a result of the redistribution of Cr and N at the α/γ -phase boundary.

When DSS is exposed at 600-1000 $^\circ\text{C}$ for an extended interval, precipitates (e.g., Cr_2N or Cr_{23}C_6) can form during decomposition of the ferrite phase. Formation of such high-Cr-containing precipitates should result in areas locally depleted of Cr around the precipitates; this area is known to form a secondary austenite phase (γ_2) (Ref 31-33). During aging, local segregation occurred in the α/γ -phase boundary area because redistribution proceeded in the α - and γ -phases containing high amounts of Cr and N, respectively. Because of this redistribu-

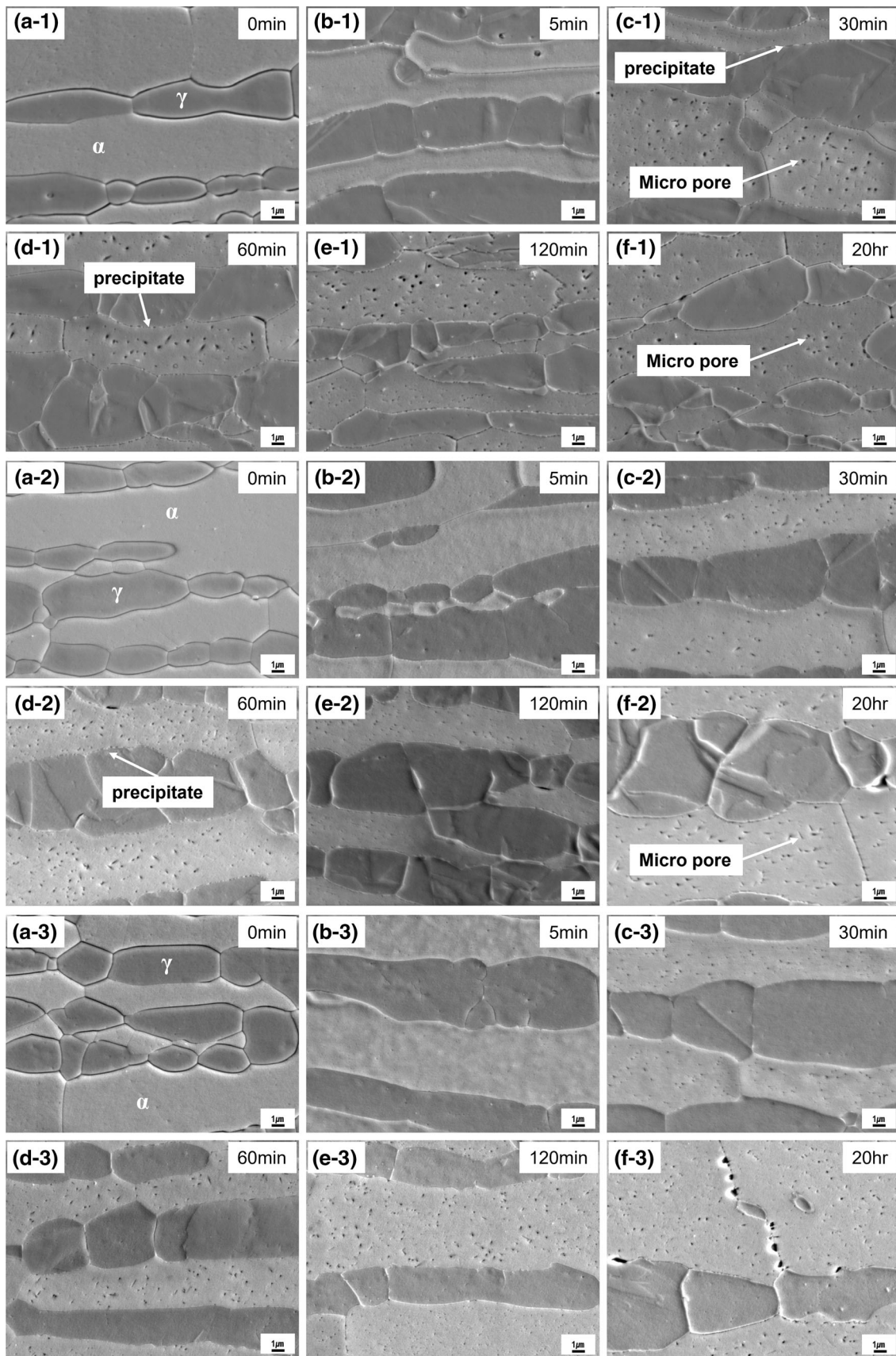


Fig. 1 Field-emission scanning electron microscope micrographs of (1) Mo-free, (2) 1Mo, and (3) 2Mo duplex stainless steels after aging at 700 °C for (a) 0, (b) 5, (c) 30, (d) 60, and (e) 120 min and (f) 20 h. (the specimens were immersed in a 4 mol/L NaCl + 0.01 mol/L HCl solution)

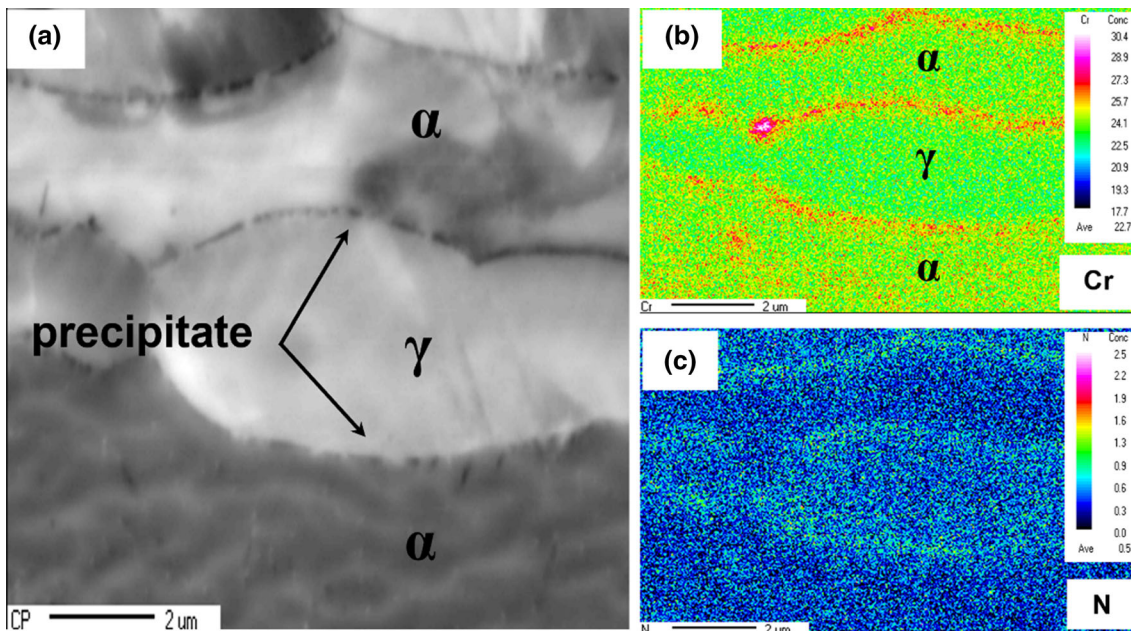


Fig. 2 (a) Backscattered electron image of the ferrite/austenite-phase boundary and elemental mapping images for (b) Cr and (c) N across the α/γ -phase boundaries in a 1Mo duplex stainless steel sample aged at 700 °C for 60 min using a field-emission electron probe microanalysis

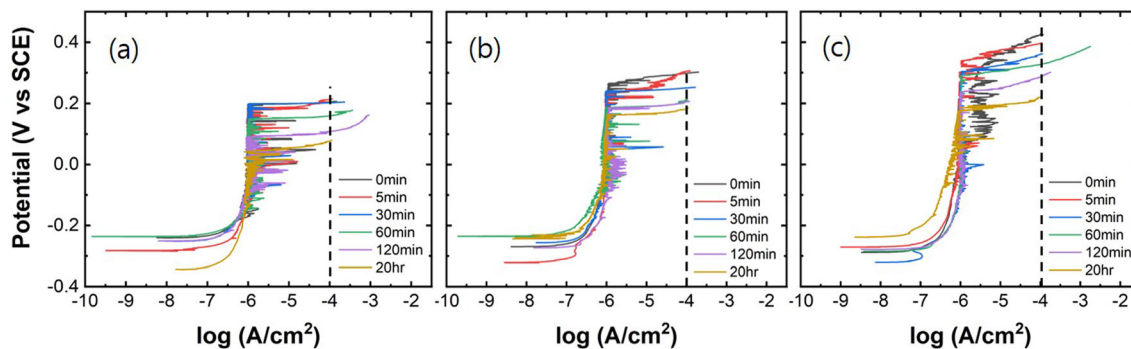


Fig. 3 Polarization curves of duplex stainless steel for different aging intervals. (a) 0Mo, (b) 1Mo, and (c) 2Mo

tion, precipitates containing high levels of Cr and N were formed, while Cr and N were diminished from the surrounding area (Ref 31). The precipitation of Cr_2N causes local compositional changes and consequently affects the stability of the surrounding α - or γ -phase. Cr depletion due to Cr_2N precipitation is expected at the α/γ -phase boundaries, thus affecting local corrosion behavior (Ref 34).

3.2 Pitting Corrosion Behavior

The PREN is one of the measurements of pitting resistance (localized corrosion) of stainless steels, calculated using Eq. 1 as follows (Ref 35, 36):

$$\text{PREN} = \% \text{Cr} + 3.3\% \text{Mo} + 30\% \text{N} - 1.0\% \text{Mn} \quad (\text{Eq 1})$$

where the concentration of the alloying element is expressed as wt.%. When Cr is 1 wt.%, the index is 1, and Mo has a 3.3-fold greater effect than does Cr. Thus, it is possible to evaluate the pitting resistance of stainless steel according to the PREN formula. Figure 3 presents potentiodynamic polarization curves of the DSS specimens measured in 3.5% NaCl solution. All the curves show similar trends with distinct active-passive transi-

tion having passivity region with constant current density in a potential range. Several current peaks in all the steel samples appeared in the passive region, indicating depassivation and repassivation. This should be caused by the surface defects such as micropores formed during solidification, inclusions or precipitates (Ref 37). It can be seen also that there are no significant differences in the corrosion current density of each sample despite of various Mo contents and different aging intervals, that is, corrosion rate among the experimental range was not significantly influenced. However, as predicted, the pitting potential (E_{pit}) which was identified as the potential where the current density reached $100 \mu\text{A}/\text{cm}^2$ increased with an increase in Mo content. With the increase in aging time, the passive potential range was reduced and E_{pit} was also decreased. The detailed results of E_{pit} from Fig. 3 are provided in Table 3, where the E_{pit} increases with Mo content and decreases significantly with aging time. However, the corrosion potential (E_c) was not distinctly influenced by Mo content and aging time.

To confirm the polarization data, the CPT of each DSS specimen was measured in 1 mol/L NaCl solution (Fig. 4 and Table 3). Figure 4(a) shows that the unaged steel (0Mo-0 min)

had a CPT of 18.6 °C, but this rapidly decreased to less than 5 °C after 5 min of aging. The CPT continuously decreased with an increase in aging time.

Figure 4(b) of 1Mo steel and Fig. 4(c) of 2Mo steel show the same trend as 0Mo steel: CPT continuously decreases with an increase in aging time. Regarding Mo-containing DSS, the decreasing rate of CPT with aging time was smaller, compared with the 0Mo steel. To corroborate the E_{pit} and CPT results, changes in E_{pit} and CPT as a function of aging time in 0Mo, 1Mo, and 2Mo steels are presented in Fig. 5. The E_{pit} and CPT values displayed similar trends. With the increase in aging time, E_{pit} and CPT values both decreased for aging time intervals of 30 min to 20 h.

3.3 Pitting and Precipitation Analysis

FE-DEM image of 1Mo DSS (Fig. 6a) shows that pits in unaged steels were present mostly in the α -phase region. Regarding DSS that had been aged for 30 min, more pits were observed at the α/γ -phase boundary than in the α -phase region. After the longest aging interval of 20 h, most pits were observed at the α/γ boundary. Figure 7 presents the area ratios of pits initiated in the α -phase and the α/γ -phase boundary areas as a function of aging time. Regarding 0Mo steel, after 0 min of aging, the relative area ratio of pits initiated in these regions was 7:3; after aging for 30 min, the ratio was reversed to 3:7. At 20 h of aging, the fraction of pits observed at the α/γ -phase boundary was 86%, which was identical in 1Mo and 2Mo steels. Thus, although pitting occurred mostly in the α -phase region in unaged steels, aging caused more pits to form at the α/γ -phase boundary.

Figure 8 presents backscattered electron images of pits after CPT testing and elemental mapping images (FE-EPMA) for Cr and N of 1Mo steel that had been aged for 0 min and 20 h.

Table 3 Pitting potentials (V) of duplex stainless steels for different aging intervals after polarization in 3.5% NaCl solution at 30 °C

Grade	0 min	5 min	30 min	60 min	120 min	20 h
0Mo	0.205	0.213	0.202	0.159	0.108	0.077
1Mo	0.298	0.305	0.250	0.211	0.206	0.182
2Mo	0.423	0.395	0.359	0.327	0.285	0.220

While pits in unaged DSS were found mostly in the α -phase region (Fig. 8a), DSS that had been aged for 20 h showed pits formed at the α/γ -phase boundary (Fig. 8b) where Cr and N were dense. This indicated that nitride-containing Cr was formed at the phase boundary. HAADF-STEM imaging indicated that the nitride came from Cr_2N (Fig. 9a). The high-resolution Z-contrast STEM could provide incoherent images, implying the possibility of an accurate characterization of the precipitates. Rod-like particles were characterized as

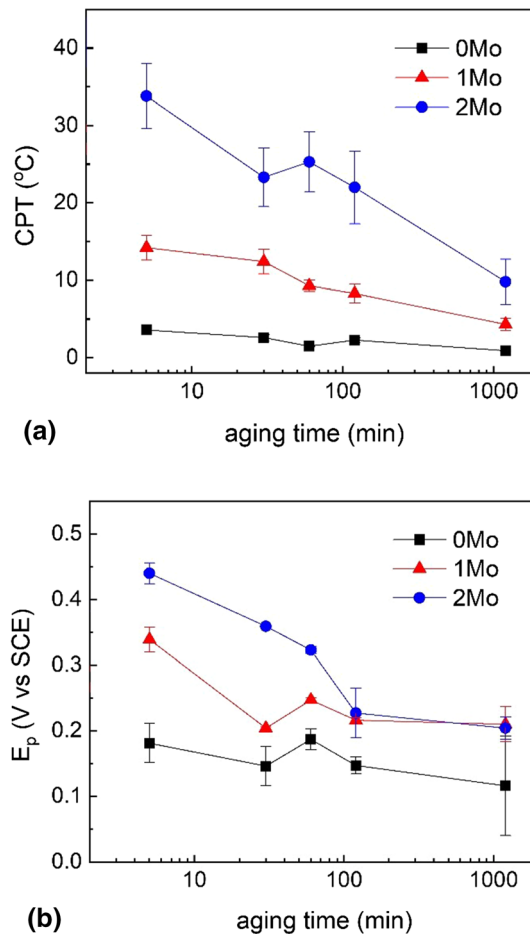


Fig. 5 Comparison of the (a) critical pitting temperature and (b) pitting potential of duplex stainless steel as a function of aging time

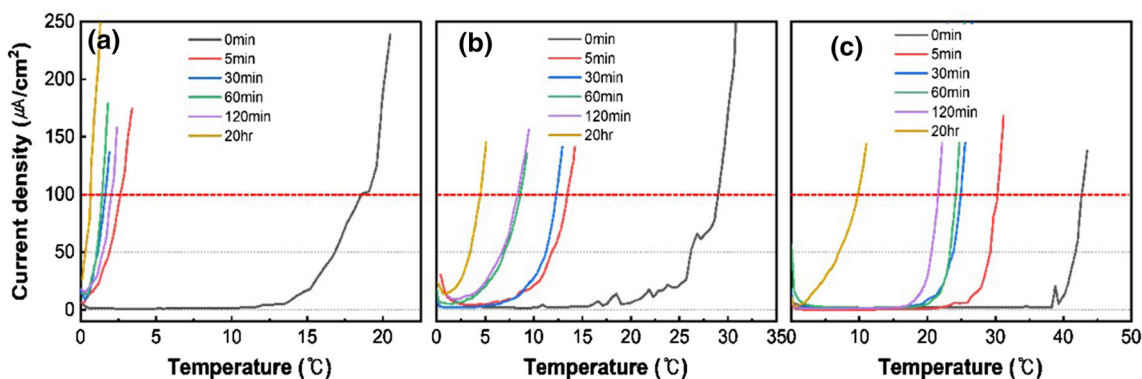


Fig. 4 Typical critical pitting temperature test curves of current density as a function of the temperature of duplex stainless steel. (a) 0Mo, (b) 1Mo, and (c) 2Mo

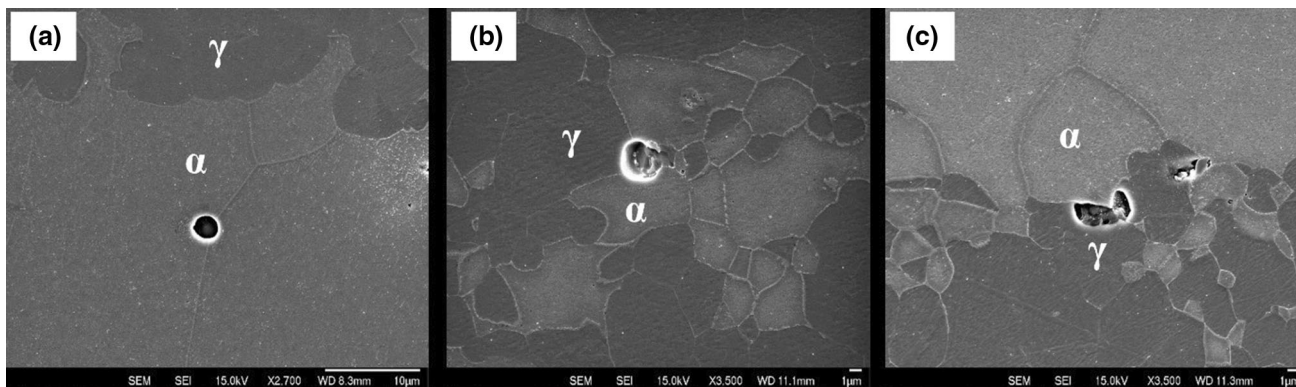


Fig. 6 Scanning electron microscopy morphologies of the corrosion pits of duplex stainless steel aged for (a) 0 min, (b) 30 min, and (c) 20 h

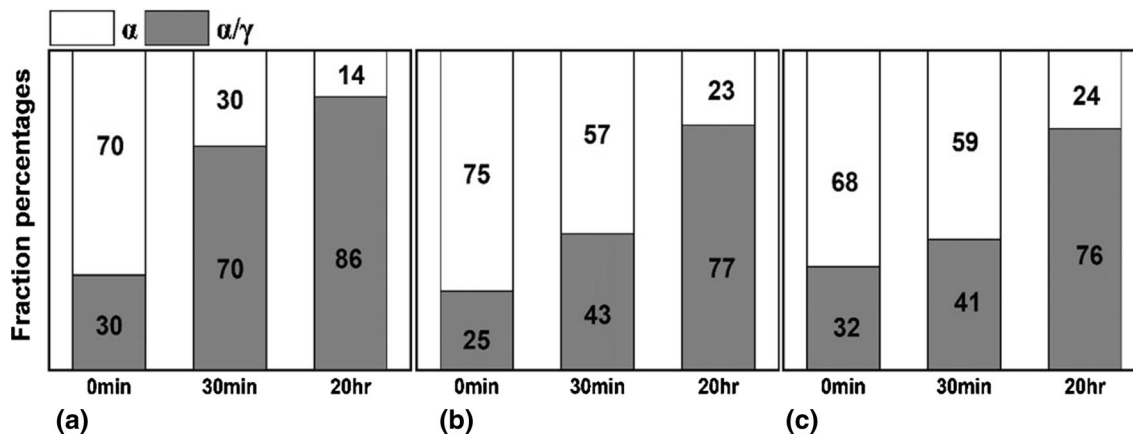


Fig. 7 Estimated area ratios of pit formation in duplex stainless steels for different aging intervals. (a) 0Mo, (b) 1Mo, and (c) 2Mo

Cr_2N precipitate (Fig. 9a), which had a hexagonal close-packed (hcp) crystal structure according to the analysis of the selected area diffraction pattern as shown in Fig. 9(b).

As previously noted, during aging, local segregation occurred in the α/γ -phase boundary area, where the redistribution of Cr and N components occurred, resulting in the localized precipitation of Cr_2N . When precipitates containing high levels of Cr and N are formed, Cr and N components are depleted near the α/γ -phase boundary area (Ref 32). Table 4 lists the equilibrium chemical composition of α - and γ -phases determined by Thermo-Calc software and calculated PRENs. Before aging, pits preferentially formed in the α -phase (Fig. 7) because of the lower PREN of the α -phase, compared with the PREN of the γ -phase (Ref 26, 38, 39). After aging, numerous Cr_2N precipitates formed at the α/γ -phase boundary. This should have led to much lower PRENs around the precipitates because of Cr depletion, followed by the formation of more pits at the boundary as aging time increases. This mechanism is shown in Fig. 10, where the Cr-depleted zone formed in the vicinity of Cr_2N precipitates acted as preferentially the initiation site of pit. We attempted to analyze the composition of the tiny depleted zone, but the precise composition of Cr and other elements could not be determined. Nevertheless, we presume that the PREN of this zone in an aged sample was much lower than the PREN in an unaged sample. Magnabosco (Ref 40) reported that there was a reduction in pitting potential with an increase in the degree of depletion of Cr and Mo, which made possible the assessment of the localized corrosion

resistance of ages 2205 DSS through simulation of σ -phase formation using by composition profiles. The reduction in E_p by the σ -phase formation in the work (Ref 40) was much higher compared with by Cr_2N formation in this study, because E_p of unaged 2205 DSS was higher than that of lean DSS and σ -phase could form higher degree of depletion of the Cr and Mo elements compared with Cr_2N (Table 5).

4. Summary

The effects of Mo addition and aging of 21Cr lean DSS on pitting corrosion resistance were investigated. Key findings of the research were as follows:

1. The E_{pit} values were in good agreement with measured CPTs. Pitting resistance improved with an increase in Mo content.
2. Aging at 700 °C caused local segregation in the area of α/γ -phase boundary where the redistribution of Cr and N components occurred. This led to the precipitation of a second phase, identified as Cr_2N , which resulted from depletion of Cr and N near the boundary.
3. The E_{pit} and CPT values decreased rapidly with an increase in aging time. Thus, aging lowered the pitting corrosion resistance.

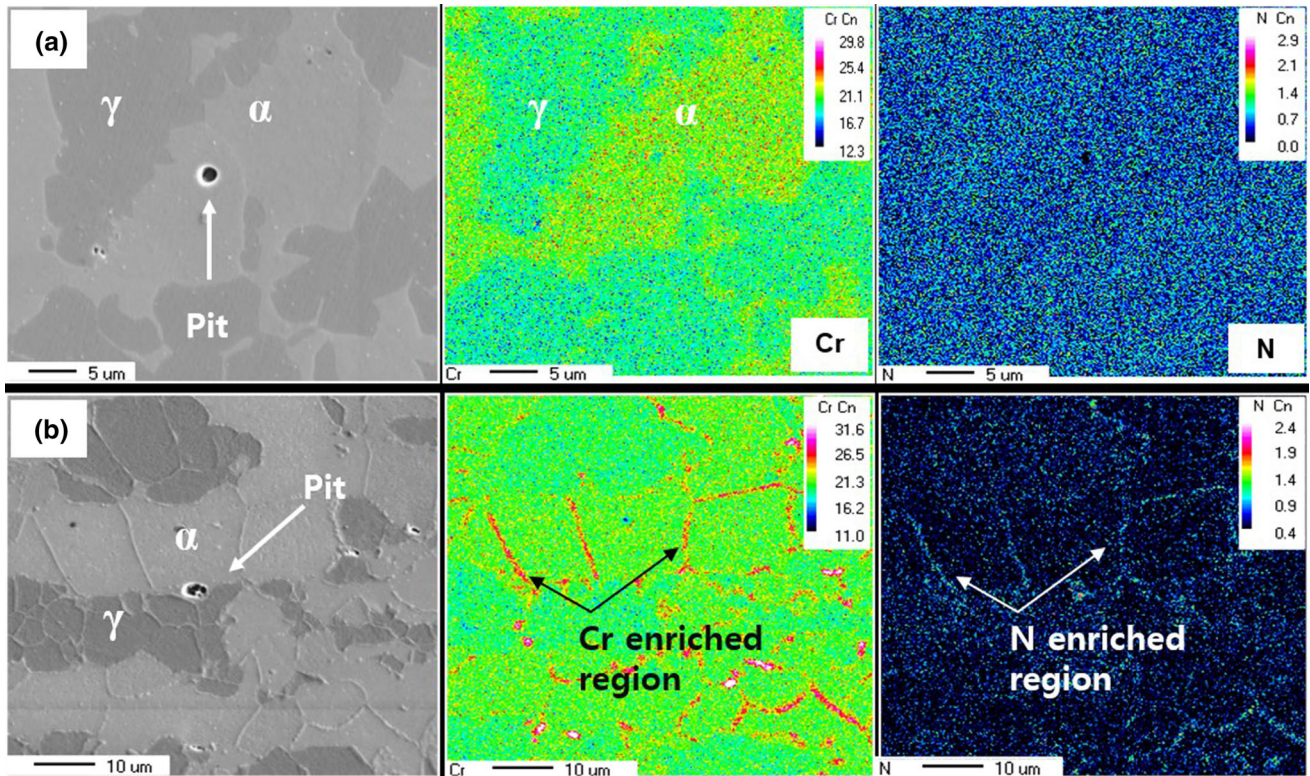


Fig. 8 Backscattered electron images of pits after critical pitting temperature testing, and field-emission electron probe microanalysis distribution elemental mapping images for Cr and N, of 1Mo steel aged for (a) 0 min and (b) 20 h

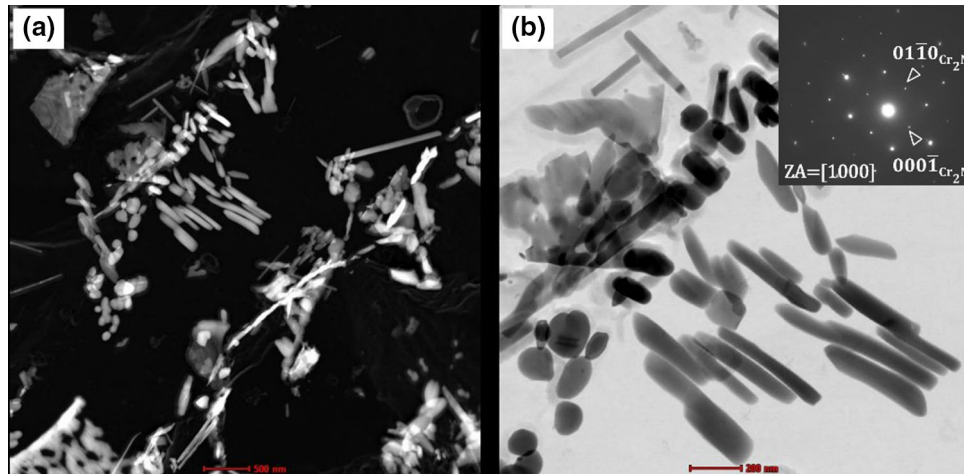


Fig. 9 Images of Cr_2N precipitates (a) on carbon replicas using a HAADF-STEM, and (c) STEM-BF and selected area diffraction pattern (SADP) in 1Mo sample after aging at 700 °C for 60 min

Table 4 Critical pitting temperatures (°C) of duplex stainless steels aged for different times

Grade	0 min	5 min	30 min	60 min	120 min	20 h
0Mo	18.6	2.9	1.7	1.6	2.2	0.7
1Mo	29.2	13.6	12.5	8.9	8.4	4.7
2Mo	43.0	30.7	25.4	24.3	21.9	9.8

- Pitting occurred mostly in the α -phase region in unaged DSSs, whereas more pits were observed at the α/γ -phase boundary after aging because of Cr depletion around boundaries associated with the precipitation of high-Cr-containing species, such as Cr_2N .

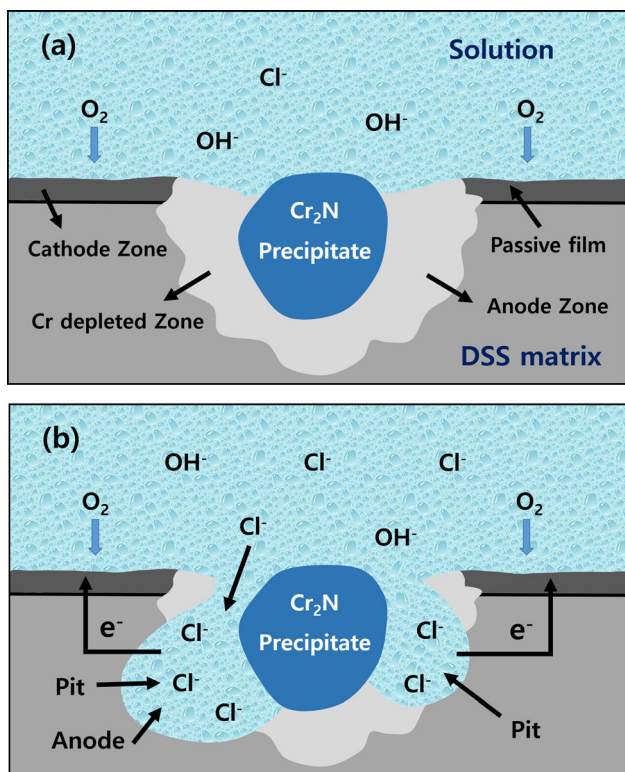


Fig. 10 Schematic diagrams of pitting corrosion mechanism of DSS at the Cr-depleted zone in the vicinity of Cr₂N precipitates

Table 5 Chemical compositions (wt.%) and pitting resistance equivalent numbers (PRENs) of α - and γ -phases of duplex stainless steels calculated using Thermo-Calc software v.10 and the database (TCFE6.2)

Grade	Phase	Cr	Mo	Ni	Mn	N	PREN
0Mo	α	23.7	...	0.70	3.20	0.044	21.82
	γ	19.6	...	1.18	3.90	0.274	23.92
1Mo	α	23.0	1.20	0.73	3.20	0.047	25.17
	γ	19.6	0.80	1.22	3.90	0.324	28.06
2Mo	α	22.5	2.40	0.75	3.30	0.051	28.65
	γ	19.80	1.60	1.25	4.10	0.401	33.01

References

1. Y. Chen, B. Yang, Y. Zhou, Y. Wu and H. Zhu, Evaluation of Pitting Corrosion in duplex stainless steel Fe20Cr9Ni for Nuclear Power Application, *Acta Mater.*, 2020, **197**, p 172–183
2. J. Charles, and P. Chemelle, in: Proceedings of the 8th Duplex Stainless Steels, Baunne, France, 2010, p 29–82
3. X. Zhang et al., Microstructure and Mechanical Properties of TOP-TIG-Wire and Arc Additive Manufactured Super Duplex Stainless Steel (ER2594), *Mater. Sci. Eng. (A)*, 2019, **762**, p 138097. <https://doi.org/10.1016/j.msea.2019.138097>
4. R. Gunn, ed. Duplex Stainless Steels: Microstructure, Properties and Applications. Woodhead Publishing, 1997
5. L. Pezzato et al., Effect of the Heat Treatment on the Corrosion Resistance of Duplex Stainless Steels, *J. Mater. Eng. Perform.*, 2018, **27**(8), p 3859–3868
6. M. Breda, L. Pezzato, M. Pizzo, and I. Calliari, Effect of Cold Rolling on Pitting Resistance in Duplex Stainless Steels, *La Metallurgia Italiana* - n. 6/2014

7. Y. Wang, H. Sun, N. Na, Y. Xiong, and H. Jing, Effect of Sigma Phase Precipitation on the Pitting Corrosion Mechanism of Duplex Stainless Steels, *Int. J. Electrochem. Sci.*, 2018, **13**, p 9868–9887. <https://doi.org/10.20964/2018.10.38>
8. S. Ishikawa, T. Yamashita, T. Kiryu, Y. Chai and Y. Kimura, Effect of Mo Addition on Laves Phase Precipitation Behavior in Fe-20% Cr-x% Nb Alloys, *Mater. Charact.*, 2022, **190**, p 112077. <https://doi.org/10.1016/j.matchar.2022.112077>
9. L. Karlsson, S. Rigdal, and F. Lake, Proceedings of Duplex America 2000, Houston, USA, 2000, pp. 257–272
10. J.-O. Nilsson, A. Wilson, B. Josefsson, and T. Thorvaldsson, Proceedings of the Applications of Stainless Steel 1992, Stockholm, Sweden, 1992, p 280–289
11. S. Hertzman, B. Lehtinen, and E. Symniotis-Barrdahl, Proceedings of the Applications of Stainless Steel 1992, Stockholm, Sweden, 1992, p 345–359
12. L. Liao, J. Li, F. Xu, and W. Zhang, Role of Substitution of Ni by Co During Isothermal Aging of Superaustenitic Stainless Steels: Precipitation Behavior and Phase Transformations, *Metall. Mater. Trans. A*, 2022, **53**(6), p 2130–2145.
13. H.Y. Ha, T.H. Lee, C.G. Lee, and H.M. Yoon, Understanding the Relation between Pitting Corrosion Resistance and Phase Fraction of S32101 Duplex Stainless Steel, *Corros. Sci.*, 2019, **149**, p 226–235. <https://doi.org/10.1016/j.corsci.2019.01.001>
14. J.-O. Nilsson, Super Duplex Stainless Steels, *Mater. Sci. Technol.*, 1992, **8**(8), p 685–700.
15. T.H. Chen, K.L. Weng, and J.R. Yang, The Effect of High-Temperature Exposure on the Microstructural Stability and Toughness Property in a 2205 Duplex Stainless Steel, *J. Mater. Sci. Eng. A*, 2002, **338**(1–2), p 259–270.
16. D.M. Escriba Villanueva et al., Comparative Study on Sigma Phase Precipitation of Three Types of Stainless Steels: Austenitic, Superferritic and Duplex, *Mater. Sci. Technol.*, 2006, **22**(9), p 1098–1104.
17. J.H. Park, and H.S. Kwon, Development of High Mn–N Duplex Stainless Steel for Automobile Structural Components, *Corros. Sci.*, 2008, **50**(2), p 404–410.
18. T. Laitinen, L. Wegelius, and A. Bergquist, Mill Exposure Test of Duplex Stainless Steel LDX 2101 in Recycled Fiber Applications, 6th Stainless Steel Conference, Helsinki, Finland, 2008, pp. 599–604
19. K. Sugimoto, and Y. Sawada, The role of molybdenum additions to austenitic stainless steels in the inhibition of pitting in acid chloride solutions, *Corros. Sci.*, 1977, **17**(5), p 425–445.
20. J. Moon, H. Ha, S. Park, T. Lee, and J. Jang, Effect of Mo and Cr Additions on the Microstructure, Mechanical Properties and Pitting Corrosion Resistance of Austenitic Fe-30Mn-10.5 Al-1.1 C Lightweight Steels, *J. Alloys Compnd.*, 2019, **775**, p 1136–1146.
21. Y.C. Lu, M.B. Ives, and C.R. Clayton, Synergism of Alloying Elements and Pitting Corrosion Resistance of Stainless Steels, *Corros. Sci.*, 1993, **35**(1–4), p 89–96.
22. J.D. Henderson, X. Li, D.W. Shoosmith, J.J. Noel, and K. Ogle, Molybdenum Surface Enrichment and Release during Transpassive Dissolution of Ni-Based Alloys, *Corros. Sci.*, 2019, **147**, p 32–40.
23. R.C. Newman, The Dissolution and Passivation Kinetics of Stainless Alloys Containing Mo-II: Dissolution Kinetics in Artificial Pits, *Corros. Sci.*, 1985, **25**(5), p 341–350.
24. M. Kaneko, and H.S. Isaacs, Effects of Mo on the Pitting of Ferritic- and Austenitic-Stainless Steels in Bromide and Chloride Solutions, *Corros. Sci.*, 2002, **44**(8), p 1825–1834.
25. A.J. Ramirez, J.C. Lippold, and S.D. Brandt, The Relationship between Chromium Nitride and Secondary Austenite Precipitation in Duplex Stainless Steels, *Metall. Mater. Trans. A*, 2003, **34**(8), p 1575–1597.
26. L. Zhang et al., Effect of Aging on the Corrosion Resistance of 2101 Lean Duplex Stainless Steel, *Mater. Charact.*, 2009, **60**(12), p 1522–1528.
27. L.-C. An et al., Effects of Mo and Mn on Pitting Behavior of Duplex Stainless Steel, *J. Iron Steel Res. Int.*, 2016, **23**(12), p 1333–1341.
28. C. Pareige et al., Kinetics of G-Phase Precipitation and Spinodal Decomposition in VERY LONG AGED FERRITE of a Mo-Free Duplex Stainless Steel, *J. Nucl. Mater.*, 2015, **465**, p 383–389.
29. J.Y. Choi, and K.T. Park, Secondary Austenite Formation during Aging of Hot-Rolled Plate of a TRIP-Aided Mo-Free Lean Duplex Stainless Steel, *Met. Mater. Int.*, 2020 <https://doi.org/10.1007/s12540-020-0068-9-7>

30. B.J. Yoon, and Y.S. Ahn, Effect of Mo Addition on Aging Behavior of TRIP-Aided Duplex Stainless Steel, *Mater. Charact.*, 2021, **173**, p 110946.
31. D.Y. Kobayashi, and S. Wolyneec, Evaluation of The Low Corrosion Resistant Phase Formed during the Sigma Phase Precipitation in Duplex Stainless Steels, *Mater. Res.*, 1999, **2**(4), p 239–247.
32. M. Liljas, P. Johansson, H.-P. Liu, and C.-O.A. Olsson, Development of a Lean Duplex Stainless Steel, *Steel Res. Int.*, 2008, **79**(6), p 466–473.
33. J.Y. Maetz, S. Cazottes, C. Verdu, and X. Kleber, Precipitation and Phase Transformations in 2101 Lean Duplex Stainless Steel during Isothermal Aging, *Metall. Mater. Trans. A*, 2016, **47**(1), p 239–253.
34. Magnabosco et al., Use of Composition Profiles Near Sigma Phase for Assessment of Localized Corrosion Resistance in a Duplex Stainless Steel, *Calphad*, 2019, **64**, p 126–130.
35. H. Vannevik et al., Effect of Elemental Partitioning on Pitting Resistance of high nitrogen duplex stainless Steels, *ISIJ Inter.*, 1996, **36**, p 807–812.
36. L. Weber, and P.J. Uggowitzer, Partitioning of Chromium and Molybdenum in Super Duplex Stainless Steels with Respect to Nitrogen and Nickel Content, *Mater. Sci. Eng. A*, 1998, **242**, p 222–229.
37. C.-J. Park, H.-S. Kwon, and M.M. Lohrengel, Micro-Electrochemical Polarization Study on 25% Cr Duplex Stainless Steel, *Mater. Sci. Eng. A*, 2004, **372**(1–2), p 180–185. <https://doi.org/10.1016/j.msea.2003.12.013>
38. Z. Lihua et al., Influence of Annealing Treatment on the Corrosion Resistance of Lean Duplex Stainless Steel 2101, *Electrochem. Acta*, 2009, **54**, p 5387–5392.
39. J.O. Nilsson et al., Mechanical Properties, Microstructural Stability and Kinetics of σ -Phase Formation in 29Cr–6Ni–2Mo–0.38N Superduplex Stainless Steel, *Metall. Mater. Trans. A*, 2000, **31A**, p 35–45.
40. R. Magnabosco et al., Use of Composition Profiles Near Sigma Phase for Assessment of Localized Corrosion Resistance in a Duplex Stainless Steel, *CALPHAD-Comput. Coupling Phase Diagr. Thermochem.*, 2019, **64**, p 126–130. <https://doi.org/10.1016/j.calphad.2018.12.004>

Publisher's Note Springer Nature remains neutral with regard to jurisdictional claims in published maps and institutional affiliations.